American Mineralogist, Volume 84, pages 1049–1060, 1999

XAFS study of the coordination and local relaxation around Co^{2+}, Zn^{2+}, Pb^{2+}, and Ba^{2+} trace elements in calcite

RICHARD J. REEDER,[1,*] GERALDINE M. LAMBLE,[2] AND PAUL A. NORTHRUP[1,†]

[1]Department of Geosciences, State University of New York, Stony Brook, New York 11794-2100, U.S.A.
[2]Earth Sciences Division, Lawrence Berkeley National Laboratory, Berkeley, California 94720, U.S.A.

ABSTRACT

Analysis of divalent Co, Zn, Pb, and Ba XAFS spectra of synthetic and natural calcite samples containing trace concentrations of these heavy metals confirms their substitution in the unique Ca site in octahedral coordination with varying degrees of local distortion. The existence of each trace metal at the single site in the bulk crystal is significant in view of previous studies showing that these trace elements are incorporated differentially at multiple, structurally distinct surface sites occurring in nonequivalent growth steps on calcite surfaces. The octahedral coordination for Ba is particularly noteworthy because of its large size (35% larger than host Ca) and the fact that it rarely exists as a major constituent with such a low coordination number.

Analysis of the local distortion and relaxation around the impurities shows a nearly complete contraction of the structure around Co^{2+} and Zn^{2+}. The Co-O and Zn-O first-shell distances are only slightly longer than in $CoCO_3$ and $ZnCO_3$, with a site compliance of ~80–90%. Displacements of higher shells relative to those in calcite decrease rapidly, but irregularly, over a short distance, and the relaxation may be largely confined within 6–7 Å of the impurity. The dilation around the large Pb^{2+} and Ba^{2+} ions in calcite also shows a high degree of site compliance (85–90%). Relaxation around Pb and Ba also appears to be restricted, but extending further for Ba than for Pb. The limited observations suggest that compliance of the octahedral site in calcite is larger than for the cation site in the rocksalt structure. The high compliance for the metal site in calcite may reflect the corner-sharing topology of the structure and is also probably the reason that calcite shows such a wide range of isovalent substitutions in nature. The findings also provide a direct indication of the local strain associated with a dilute substitutional solid solution.

INTRODUCTION

The uptake and incorporation of dissolved trace metals into a mineral during growth, known as coprecipitation, has been one of the most widely studied aspects of mineral-water interactions. A primary application for such trace element studies has been the identification of fluids and environments of crystallization and diagenesis of minerals and rocks. It is now widely appreciated that coprecipitation is an important process that may control the mobility and fate of dissolved toxic and heavy-metal species in near-surface environments.

Coprecipitation of divalent metals with calcite has received considerable attention, because calcite readily forms in a wide variety of environments and tends to incorporate a broad spectrum of geochemically and environmentally important trace elements. Whereas early work focused primarily on establishing partition coefficients for various divalent metal ions, more recent works have explored the different factors that influence the magnitude of partitioning of a given trace element between solution and crystal (see reviews by Mucci and Morse 1990; Morse and Bender 1990; Rimstidt et al. 1998). Among these factors are the influence of coupled substitutions during coprecipitation (i.e., correlated partitioning for two or more trace elements incorporated simultaneously), the influence of growth rate on the partition coefficient, and the influence of surface structure and multiple surface sites on incorporation. Relatively little attention has been given to the local structural environment of the trace metals in the calcite structure beyond the most basic issue of whether a species substitutes in the Ca position. This has been partly limited by the availability of element-specific methods that provide direct structural information. Aspects such as distortion and relaxation around different trace elements and the possible existence of clustering or short-range order are fundamental for understanding both partitioning behavior and stability of dilute solid solutions, and consequently they have implications for the sequestering of toxic metals in minerals.

Direct determination of such structural aspects is now possible for individual trace elements in solids using X-ray absorption fine structure (XAFS) spectroscopy at synchrotron radiation facilities. In the present study we use XAFS spectroscopy to determine directly the local coordination environ-

*E-mail: rjreeder@sunysb.edu
†Current address: Bell Laboratories, Lucent Technologies, X15B National Synchrotron Light Source, Brookhaven National Laboratory, Upton, New York 11973, U.S.A.

ment of divalent heavy metals (Co, Zn, Pb, and Ba) coprecipitated in synthetic and natural calcite. The results allow a systematic characterization of the distortion and relaxation associated with substitution of ions that are larger and smaller than the host ion.

BACKGROUND AND SCOPE

In calcite, Ca occupies a unique octahedral site with point symmetry $\bar{3}$. Cell six Ca-O distances are identical (2.36 Å), and the CaO6 octahedron is only slightly trigonally elongated (cf. Reeder 1983). Unlike Ng^{2+}, Co^{2+}, Zn^{2+}, Fe^{2+}, and Mn^{2+}, all of which occure commonly in octahedral coordination, the larger ions Sr^{2+}, Pb^{2+}, and Ba^{2+} usually have a higher coordination number; and it is well known that $SrCO_3$, $PbCO_3$, and $BaCO_3$ form only in the aragonite structure (at ambient conditions) in which the coordination of the metal is ninefold. As an impurity, however, an ion may occur in a coordination in which it is not commonly found as a major constituent. For example, Sr substitutes readily in the Ca site of calcite, as demonstrated by a Sr *K*-edge XAFS study of selected Sr-rich calcite samples (Pingitore et al. 1992). Heterovalent ions such as U^{4+} may also substitute in the Ca site as was recently shown by the XAFS study of Sturchio et al. (1998). Pb^{2+} is also generally assumed to substitute in the Ca site of calcite even though octahedral coordination is uncommon for this ion, which often shows a preference for distorted polyhedra or off-centering, sometimes attributed to the presence of a stereoactive lone electron pair (cf. Hyde and Andersson 1989; Moore et al. 1991). In contrast, there has been some question about the coordination of Ba^{2+} in calcite. Ba is ~35% larger than Ca, and it usually has a coordination number of 8–12 when present as a major constituent. On the basis of coprecipitation systematics Pingitore (1986) tentatively concluded that Ba does not substitute for Ca, but rather occupies a kind of defect site. Here we are able to show that octahedral coordination is indeed possible for Ba^{2+} in calcite, although not without significant distortion.

Most molecular-scale views of partitioning behavior take some account of the difference in size between the trace element and the host ion in a bulk site in the solid. Because coprecipitation generally results in solid solutions, many solid solution models also consider ion size differences, for example through interaction parameters. The degree of structural distortion associated with such size differences is important for understanding partitioning and solid solution behavior at an atomic scale and should have some influence on model parameters. Blundy and Wood (1991, 1994) applied this idea to trace-element partitioning behavior between melts and crystals by considering the elastic strain associated with substitution. Gnanapragasam and Lewis (1995) also incorporated a term for elastic strain in accounting for Ra^{2+} partitioning into various calcium salts. Localized dilation or contraction around one trace element has also been considered to have an influence on the partitioning behavior of other trace elements (cf. Kitano et al. 1971; Mucci and Morse 1983; Busenberg and Plummer 1985; see also Mucci and Morse 1990 and references therein).

Such distortions are reflected by the interatomic distances in the immediate environment of the impurity and can be determined directly by XAFS spectroscopy. In contrast, X-ray diffraction averages over all atoms at a given site in a crystal and hence provides average interatomic distances; for a dilute solid solution, an average M-O distance is usually very similar to that for the pure host and hence provides little information about the local environment of the impurity.

From growth experiments involving aqueous solutions, Paquette and Reeder (1990, 1995) and Reeder (1996) suggested that coordination and geometry of surface sites might be more important than bulk sites in controlling the partitioning behavior. Evidence was found for the existence of multiple, structurally distinct surface sites in nonequivalent growth steps on the $\{10\bar{1}4\}$ face of calcite; incorporation of divalent metals with sizes larger than Ca were preferentially incorporated into one set of growth steps, whereas metals smaller than Ca, except for Zn, are preferentially incorporated into the nonequivalent set. The step-selective incorporation trend of Zn^{2+} was the same as the divalent ions larger than Ca (Reeder 1996), but no explanation for this anomalous behavior was identified.

The present study addresses whether trace metal incorporation at multiple, structurally distinct surface sites results in different coordination environments within the bulk, even though the different surface sites correspond to a single site in the bulk. We study Zn for its seemingly anomalous behavior (Reeder 1996) and explore whether atoms of a given trace metal may be clustered within the bulk, such that nearest metal neighbors are the same atom, rather than host Ca.

We chose Pb and Ba for the reasons discussed above. Co was included for comparison with Zn because their ion sizes (0.74 Å for Zn^{2+} and 0.745 Å for Co^{2+}; Shannon 1976) are nearly identical but their incorporation preferences on the calcite surface differ (Reeder 1996). Calcite samples were synthesized by the same methods as in previous work; when available, samples from the original coprecipitation experiments of Reeder (1996) were used. Local coordination of the same trace metals in natural calcite samples were measured to determine whether the local coordination differed from our synthetic samples. These four trace elements have ionic radii significantly different from Ca, and hence are also well suited for a comparison of the relative distortions required to accommodate them.

MATERIALS AND EXPERIMENTAL METHODS

Synthetic metal-doped calcite samples

Calcite single crystals (up to 500 μm) were grown from Ca-NH_3-CO_3-Cl aqueous solutions at room temperature as described by Paquette and Reeder (1995) and Reeder (1996). A given solution was doped with a single divalent metal species (Co, Zn, Pb, or Ba) as an aqueous chloride salt, which was incorporated into the calcite during growth. Heavy metal concentrations were sufficiently low so that the calculated saturation state for the respective metal carbonate was not exceeded.

Crystals used for XAFS spectroscopy were removed from growth solutions, rinsed with deionized water to remove any metals adsorbed to the surface, and dried. This procedure, combined with the relatively low total surface area of the single crystals, ensures that the XAFS signal is due entirely to the absorber in the bulk crystal, and not bound on the surface.

Inclusion-free, clear crystals were hand-picked under a microscope, finely ground in a pestle and mortar in alcohol or

acetone, and allowed to dry. Powder XRD patterns showed no indication of a second phase.

Concentrations of the divalent metals of interest were analyzed by synchrotron X-ray fluorescence microanalysis (SXRFMA) at NSLS (beamline X-26A) using multiple single crystals and the methods described by Reeder (1996). Inasmuch as the synthetic samples were chosen because of their surface-controlled differential incorporation patterns, it is an oversimplification to report a unique concentration for a given sample. Nevertheless, for simplicity we report concentrations for the synthetic samples that are averages of the high and low concentration regions (Table 1).

Natural samples and model compounds

Natural heavy-metal-containing calcites included samples from Bou Azzer, Morocco, and Peramea, Spain (Co); Franklin, NJ (Zn and Pb), Tsumeb, Namibia (Pb), and Långban, Sweden (Ba). Absorber metal concentrations were determined by SXRFMA or EPMA and are listed in Table 1.

At least two model compounds were used for each element. These included Zn^{2+}: synthetic ZnO and natural $ZnCO_3$ (smithsonite) from Kelly Mine, NM; Co^{2+}: synthetic CoO and $CoCO_3$; Pb^{2+}: synthetic tetragonal (i.e., red) PbO and natural $PbCO_3$ (cerrusite) from Tsumeb, Namibia; and Ba^{2+}: synthetic $BaCO_3$ and $BaSO_4$. All model compounds were checked by powder XRD to confirm their identity and to determine whether any second phase material was present.

XAFS experiments and analysis

All XAFS spectra were collected at beamline X-11A of the National Synchrotron Light Source, Brookhaven National Laboratory. Powdered samples were pressed into aluminum sample holders and sealed with Kapton tape. Spectra were collected at ~77 K to minimize anharmonicity and to improve signal/noise. *K*-edges were scanned for Co (7709 eV), Zn (9659 eV), and Ba (37441 eV). For Pb, the L_3-edge (13055 eV) was used. Scans of the Co and Zn *K*-edges utilized flat Si(111) double crystals for the monochromator, which was calibrated using the first inflection point in edge scans of Co or Zn metal foils. Scans of the Ba *K*-edge used Si(311) monochromator crystals, and the first inflection point of the edge from $BaCO_3$ was assigned the energy 37441 eV. Pb L_3-edge scans utilized Si(111) and Si(311) monochromator crystals in separate sessions and the first inflection point was assigned a value of 13035 eV. The energy resolution at the edges of interest was approximately 1–1.5 eV. Higher order harmonics were rejected by detuning one monochromator crystal (typically 30–40%) until the harmonic contribution was negligible.

TABLE 1. Average absorber trace element concentrations in calcite samples used for XAFS spectroscopy

Calcite	Atom (ppm)
Co	
Synthetic (2/15/95-2)	2150
Synthetic (7/5/94-1)	375
Natural (Peramea, Spain)	5800
Zn	
Synthetic (7/5/94-3)	945
Synthetic (2/1/94-1)	260
Natural (Franklin, N.J.)	245
Ba	
Synthetic (9/27/95-1)	2125
Natural (Långban, Sweden)	1600
Pb	
Synthetic (9/27/95-3)	615
Natural (Tsumeb, Namibia)	6550
Natural (Franklin, N.J.)	735

Absorption spectra for the dilute, heavy-metal-containing calcite samples were obtained by monitoring the fluorescence yield using a Canberra 13-element Ge solid-state detector. Multiple scans (typically 8–15) were collected for each sample and then summed.

XAFS spectra for model compounds were obtained in transmission mode. Powder samples of the model compounds were mixed with boron nitride in proportions to achieve an edge step corresponding to $\ln(I_0/I) \approx 1$–1.5. Three to five scans were obtained for each sample (at ~77 K) in transmission mode and then summed.

Background subtraction utilized a modified cubic spline method. Data were then normalized and converted to *k*-space. Background-subtracted, normalized XAFS data were fitted in *R*-space using the program FEFFIT (Newville et al. 1995) with backscattering amplitudes and phase shifts calculated from the program FEFF6 (Rehr et al. 1992; Zabinsky et al. 1995). Fitting used both the imaginary and real parts of the Fourier transforms and minimized the difference between the background-subtracted, normalized data and the model $\chi(R)$, where $\chi(R)$ is the Fourier transform calculated from $\chi(k)$ by FEFF6. *R*-space windows were generally set at 0.5–4.1 Å depending on the optimum position of the minimum. The *k*-space windows were approximately 3.1–15.4 $Å^{-1}$, except in one cases in which k_{max} was reduced to ~12 $Å^{-1}$. E_0 was treated as a variable parameter during fitting. For the Ba-containing samples a slight adjustment in E_0 was allowed for the Ba-O shell, as was found to be necessary in the Ba XAFS work by Haskel et al. (1995). The amplitudes and phase shifts calculated using FEFF6 were checked by fitting at least two model compounds for each absorber. Multiple-scattering paths, consistent with the calcite structure, were considered in the fitting procedure, and their contributions were evident for the Co- and Zn-containing calcites, but not for Ba- and Pb-containing samples. Errors for the fit parameters were estimated on the basis of agreement between fitted and reported values for well-characterized model compounds, with consideration of signal-to-noise ratio, data range, and quality of fit. Typical errors for *R* are ±0.02 Å for the first shell and ±0.03–0.04 Å for higher shells. Coordination number and the Debye-Waller-type factor (σ^2) are correlated; for CN, a typical error is 20%, or approximately ±1 atom. Errors for σ^2 are roughly 0.01 $Å^2$.

RESULTS

Co^{2+} in calcite

Background-subtracted raw Co *K*-edge XAFS spectra of the synthetic and the natural Co-containing calcite are similar (Fig. 1). The spectrum (not shown) for a second synthetic sample containing 375 ppm Co is the same as for the higher concentration sample but with poorer signal-to-noise. These spectra are distinct from the $CoCO_3$ spectrum, which precludes the presence

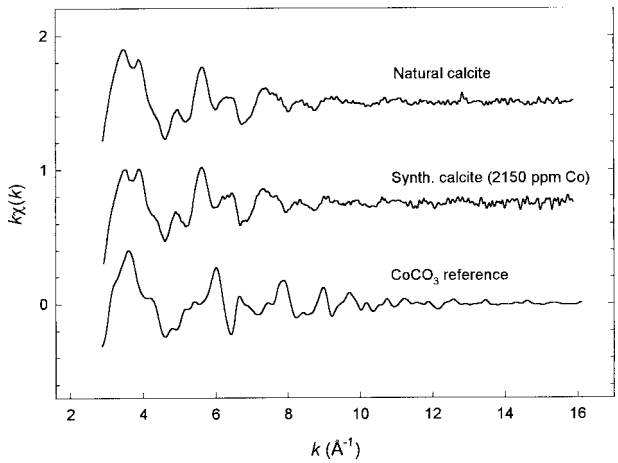

FIGURE 1. The *k*-weighted, background-subtracted raw Co *K*-edge XAFS data for Co-containing calcite samples and $CoCO_3$. Refer to Table 1 for sample information.

of a minor $CoCO_3$ impurity in the synthetic samples and is consistent with previous TEM and electron diffraction observations (Reeder 1996) indicating no second-phase inclusions.

Best fits for the Co-containing calcite samples yielded shells readily associated with the calcite structure. Table 2 gives fit parameters for both the synthetic and natural samples, which show nearly identical values, confirming a similar local environment for Co in both. (We report fit results only for the higher concentration synthetic sample because of its better signal-to-noise ratio.) For both spectra, contributions from one multiple scattering path (O-C) were found to be important. This was not indicated in a report of preliminary findings (Lamble et al. 1997), which gave only single shell fits. The first shell consists of oxygen atoms with coordination number (CN) 5.6–6.1 (±1) at a distance (*R*) of 2.14–2.16 Å (±0.02 Å). The relatively small σ^2 value (0.007 $Å^2$) indicates no significant disorder among the distances in this shell and is similar to the value found for the $CoCO_3$ model compound. The distance ~2.15 Å is only slightly greater than Co-O distances in octahedrally coordinated Co^{2+} compounds as determined by X-ray diffraction methods [e.g., 2.110 Å in $CoCO_3$ (Pertlik 1986) and 2.132 Å in CoO (Sasaki et al. 1979)]. This distance and the CN value near 6 confirm that Co occupies the unique Ca site as anticipated. The CN and *R* values determined for more distant shells support this finding. Table 3 gives distances for coordination shells of Ca out to approximately 4 Å in pure calcite. These may be compared with the shells identified by fitting the spectra of the Co-containing calcites. Co-X distances (*R*) are shorter than those in calcite, but the number of coordinating atoms as well as their identity are consistent with the shells in calcite. For example, the most distant shell modeled consists of approximately six Ca atoms (5.6–5.8) at a distance of 3.93–3.97 Å. This corresponds to the shell of the nearest Ca neighbors, which in pure calcite is composed of six Ca atoms at a distance of 4.048 Å (cf. Table 3). The shorter distances around Co are consistent with its smaller size relative to Ca. These distances contain much information about the structural response of the calcite structure for accommodating the smaller Co^{2+} ion, an aspect we consider in detail later.

No Co-Co backscattering was identified, which would be expected only if Co were strongly clustered in the structure or

TABLE 2. XAFS fit parameters for trace metal-containing calcite samples

Shell	CN	*R* (Å)	σ^2 ($Å^2$)	Shell	CN	*R* (Å)	σ^2 ($Å^2$)
	Synthetic Co^{2+}-doped calcite†				**Natural Co^{2+}-bearing calcite‡**		
O	5.6	2.16	0.007	O	6.1	2.14	0.006
C	6.0	3.12	0.009	C	5.4	3.10	0.009
O-C*	17.3	3.28	0.022	O-C*	11.2	3.14	0.030
O	6.0	3.45	0.018	O	6.7	3.44	0.006
Ca	5.6	3.97	0.005	Ca	5.8	3.93	0.007
	Synthetic Zn^{2+}-doped calcite§				**Natural Zn^{2+}-bearing calcite‖**		
O	6.4	2.15	0.008	O	6.1	2.14	0.008
C	5.6	3.13	0.017	C	6.6	3.14	0.015
O-C*	12.3	3.20	0.029	O-C*	13.4	3.22	0.031
O	5.5	3.41	0.010	O	6.1	3.41	0.010
Ca	5.3	3.94	0.004	Ca	6.0	3.94	0.006
	Synthetic Ba^{2+}-doped calcite#				**Synthetic Pb^{2+}-doped calcite****		
O	5.8	2.68	0.005	O	5.9	2.52	0.009
C	9.6	3.41	0.007	C	5.8	3.28	0.005
O	7.2	3.71	0.014	O	7.2	3.79	0.064
Ca	7.3	4.19	0.007	Ca	5.5	4.09	0.005
	Natural Pb^{2+}-bearing calcite††				**Natural Pb^{2+}-bearing calcite‖**		
O	6.4	2.51	0.009	O	6.9	2.52	0.009
C	5.7	3.28	0.010	C	4.9	3.28	0.003
O	3.8	3.72	0.060	O	3.8	3.85	0.069
Ca	5.7	4.07	0.004	Ca	5.8	4.08	0.005

* Multiple-scattering path. See text for description of estimated errors.
† 2/15/95-2. # 9/27/95-1.
‡ Peramea, Spain. ** 9/27/95-3.
§ 7/5/94-3. †† Tsumeb, Namibia.
‖ Franklin, N.J.

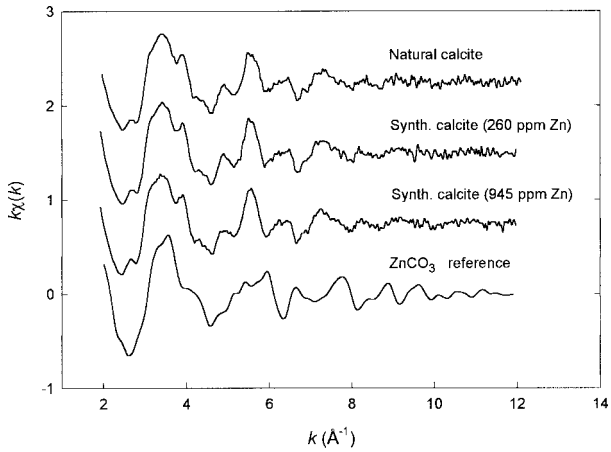

FIGURE 2. The *k*-weighted, background-subtracted raw Zn *K*-edge XAFS data for Zn-containing samples. Refer to Table 1 for sample information.

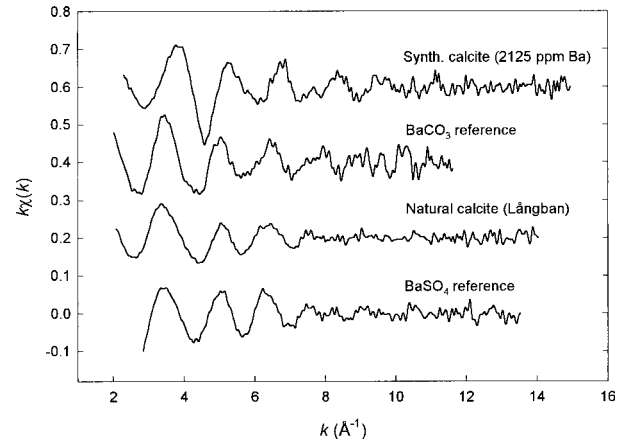

FIGURE 4. The *k*-weighted, background-subtracted raw Ba *K*-edge XAFS data for synthetic and natural Ba-containing calcites and $BaCO_3$ and $BaSO_4$ model compounds. Refer to Table 1 for sample information.

present as a discrete Co compound (e.g., $CoCO_3$). On this basis, and also because the total Co concentration in the calcites is low, we conclude that the Co is present in a dilute substitutional solid solution, even if its concentration is not uniform throughout the sample. Therefore, despite the differential incorporation of Co at nonequivalent steps, the Co has only a unique local environment in the bulk structure following incorporation.

Zn^{2+} in calcite

Results for the Zn^{2+}-containing samples are remarkably similar to those for Co^{2+}, despite the noted difference in surface-site preferences. The natural and synthetic Zn-containing calcite samples show similar XAFS, but different than that for $ZnCO_3$ (Fig. 2), confirming that the incorporated Zn is not present as a $ZnCO_3$ impurity phase. Fitting of the Zn-containing calcite spectra yields values for CN, *R*, and Debye-Waller-type factors (Table 2) that are similar within errors for the synthetic and natural samples, so that Zn has similar local environments in each. A contribution from one multiple-scattering path (O-C) was found to be important. Figure 3[1] shows the multi-shell fit to raw data for a synthetic Zn-doped calcite. Comparison of fit parameters of the different shells with the results for Co-containing calcites and with the shells in pure calcite again demonstrate that Zn occupies the unique Ca site in calcite. The first-shell distance (Zn-O), 2.14–2.15 Å, is only slightly longer than the distance in $ZnCO_3$ (2.111 Å) and is typical for octahedral coordination. This Zn-O distance is distinctly longer than values typical of tetrahedral coordination (1.96–2.00 Å), which is sometimes preferred by Zn. Moreover, CN values of 6.4 and 6.1 (±1) for the synthetic and the natural Zn-containing samples, respectively, are consistent with octahedral coordination by oxygen. Comparison of parameters from more distant shells with results for Co-containing calcites shows a close similarity. This can be expected in view of the similar ionic radii for Co^{2+} and Zn^{2+} (0.745 and 0.74 Å, respectively, for sixfold coordination). Again, no Zn-Zn backscattering was evident, indicating that clustering is either unimportant or nonexistent in the calcites examined.

Ba^{2+} in calcite

The spectrum of the synthetic Ba-containing calcite differs from that of the natural sample from Långban (Fig. 4). Furthermore, the Långban spectrum shows a marked similarity to that of $BaSO_4$, and subsequent detailed X-ray diffraction revealed three of the strongest lines of $BaSO_4$ just above the background. The XAFS spectrum of the synthetic Ba-doped calcite also differs from the spectrum for $BaCO_3$, as expected because $BaCO_3$ has a different structure than calcite, with Ba in ninefold coordination in an irregular polyhedron. This is also evident from the Fourier transform magnitudes shown in Figure 5[1] for the synthetic Ba-doped calcite and the $BaCO_3$ model compound. A fit of the $\chi(k)$ function to raw data in *k*-space for the synthetic Ba-doped calcite (Fig. 6) yields a simple structural picture, with Ba occupying the Ca position. The first shell has 5.8 O atoms at a distance of 2.68 Å (Table 2). The reasonably small Debye-Waller-type factor for this shell ($\sigma^2 = 0.005$ Å^2) suggests little disorder among the distances. Comparison of this distance with Ba-O distances determined by X-ray diffraction is problematic because there are very few compounds with Ba truly in octahedral coordination. In BaO, which has the rocksalt structure, the Ba-O distance is 2.77 Å, some 3% longer than in the Ba-doped calcite. There is a high-temperature form of $BaCO_3$ in which Ba is in octahedral coordination in a rhombohedral structure analogous to the high-temperature form of calcite. Its Ba-O distance at high temperature is 2.662 Å (Strømme 1975), which, in spite of the high temperature, is in much closer agreement with the observed Ba-O distance in the Ba-doped calcite. The 2.68 Å first shell distance for the Ba-doped calcite is significantly shorter than the mean Ba-O

[1]For a copy of Figures 3 and 5, document item AM-99-017, contact the Business Office of the Mineralogical Society of America (see inside front cover of recent issue) for price information. Deposit items may also be available on the American Mineralogist web site (http://www.minsocam.org or current web address).

TABLE 3. Distances from M^{2+} site and coordination number for pure metal carbonate standards from diffraction data

				R (Å)	
Atom*	*R* (Å)	Atom	CN	$BaCO_3$†	$PbCO_3$‡
$CaCO_3$ (calcite)§		**$BaCO_3$ (witherite) and $PbCO_3$ (corrusite)**			
O	2.360	O1	1	2.737	2.594
C	3.213	O2	2	2.742	2.659
O	3.459	O2	2	2.817	2.678
Ca	4.048	O2	2	2.836	2.716
		O1	2	2.868	2.765
$CoCO_3$ (spherocobaltite)‖		C	1	3.209	3.089
O	2.110	C	2	3.212	3.080
C	2.966	C	1	3.621	3.438
O	3.234	C	2	3.719	3.633
Co	3.669	O2	2	4.301	4.129
		Ba or Pb	2	4.369	4.180
$ZnCO_3$ (smithsonite)†					
O	2.111	Ba or Pb	2	4.382	4.218
C	2.964				
O	3.231				
Zn	3.672				

* CN = 6 for all shells in calcite-structure carbonates.
† From X-ray structure refinement of de Villiers (1971). Space group *Pmcn*.
‡ From neutron structure refinement of Chevrier et al. (1992). Space group *Pmcn*.
§ From X-ray structure refinement of Effenberger et al. (1981).
‖ From X-ray structure refinement of Pertlik (1986).

distance (2.807 Å; range 2.74–2.87 Å, Table 3) in the orthorhombic form of $BaCO_3$ stable at ambient temperature (witherite) and with ninefold coordination of the Ba. Thus the fit parameters for the first shell of Ba in the synthetic calcite are entirely consistent with an octahedral local environment.

Fit parameters for the three successive shells, composed of carbon, oxygen, and finally Ca (Table 2), confirm that Ba resides in the unique Ca site in octahedral coordination. The distances for these shells are all longer than the corresponding shells for Ca in pure calcite (Table 3), indicating a dilation of the local environment consistent with the larger size of Ba. This relaxation of the structure around the Ba ion is considered in detail later. The CN value of 9.6 for the carbon shell is larger than the expected value of six. However, carbon is a weak backscatterer, which makes determination of CN in this shell less certain. No Ba-Ba backscattering was identified in the XAFS analysis. Unlike the Co- and Zn-doped samples, no contribution from multiple-scattering paths was evident for the Ba-doped calcite. Possibly, contraction around Co and Zn allows the oxygen positions in the first shell to retain local symmetry, whereas the large dilation around Ba moves the O atoms to lower symmetry positions.

Pb^{2+} in calcite

Given that Ba^{2+} occupies the Ca position in our synthetic Ba-doped calcite, Pb^{2+} should also occupy this site with less dilation of the structure. Although we do find that Pb^{2+} occupies the Ca site in both the natural and synthetic calcites, the fit

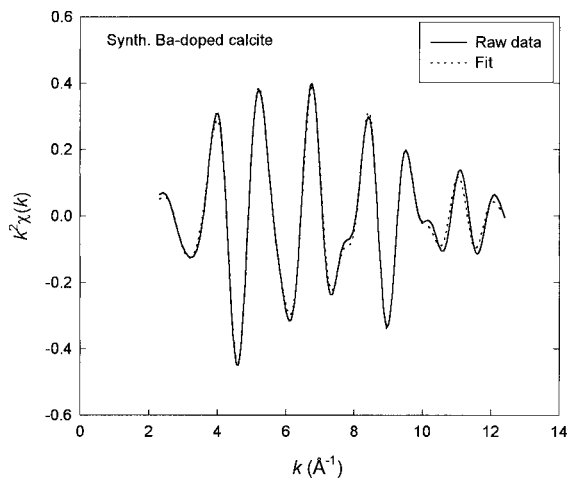

FIGURE 6. The *k*-space representation of the fit (dashed line) to the raw data (solid line) for the synthetic Ba-doped calcite. Fitting was done in *R* space.

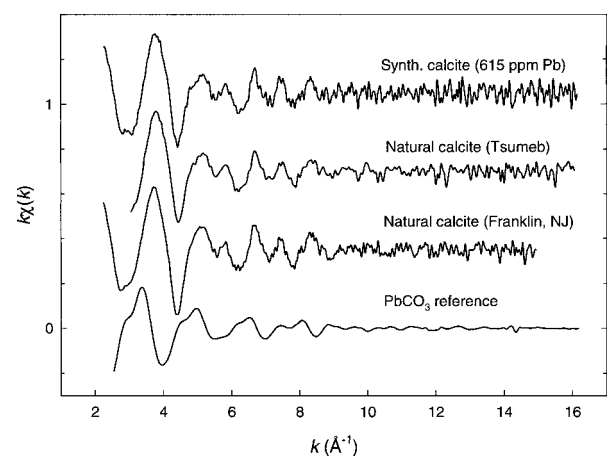

FIGURE 7. The *k*-weighted, background-subtracted raw Pb L_3-edge XAFS data for Pb-containing calcites and $PbCO_3$. Refer to Table 1 for sample information.

for the third shell (the second oxygen shell) is distinctly poor relative to the other shells. The spectra (Fig. 7) of the natural and synthetic Pb-containing calcites are nearly identical, and they are noticeably different from the spectrum for $PbCO_3$, which, like $BaCO_3$, has the orthorhombic aragonite structure, with Pb in ninefold coordination.

Fit parameters (Table 2) are similar for the synthetic and natural samples and show well-defined first (O), second (C), and fourth (Ca) shells with an arrangement similar to that for Ba-doped calcite. The fit to the third shell (i.e., the second oxygen shell) yielded large Debye-Waller-type factors (σ^2 = 0.06–0.07 Å^2) and a distance of 3.7–3.8 Å, which is distinctly longer than would be expected on the basis of the Ba results. This was found to be true for the natural Pb-containing calcite as well as the synthetic sample, with only minor differences. We collected spectra on a second natural Pb-containing sample, with nearly identical results, indicating a similar local environment for Pb in all these samples. The reason for the poor fit remains unclear. It is possible that the fit to this shell is influenced by multiple scattering, although no such contribution could be readily identified as in the cases of Co and Zn in calcite. An example of a multi-shell fit to raw data is shown in Figure 8.

Regardless of the ambiguity for this particular shell, it is evident that Pb^{2+} occupies the Ca site in calcite. First-shell fit parameters give 5.9–6.9 O atoms at 2.51–2.52 Å. These distances are only slightly shorter than values determined by X-ray diffraction for Pb^{2+} compounds with fairly regular octahedral coordination. Examples include $PbAs_2O_6$ (Losilla et al. 1995) and $PbSb_2O_6$ (Hill 1987), which have regular octahedra with Pb-O distances of 2.530 and 2.563 Å, respectively. And $PbNb_2O_6$ has slightly distorted octahedra with Pb-O distances of 2.554 and 2.598 Å (Mahe 1967). In some Pb^{2+} compounds, however, the first-shell coordination is strongly distorted or the Pb atom is shifted from the center of an irregular coordination polyhedron (e.g., orthorhombic PbO). Such effects are usually attributed to a stereochemically active lone electron pair. However, no evidence of such an effect is seen in the first shell of the Pb-containing calcites, for which the Debye-Waller-type factors are not unusually large (Table 2). Nor does it seem reasonable to suspect that the large distance for the second oxygen shell might reflect such an effect.

Fit parameters for the carbon and calcium shells give results similarly close to the Ca environment in calcite (Table 3). Moreover, these distances (the ambiguity of the second oxygen shell notwithstanding) indicate an overall dilation of the local environment around Pb, as expected on the basis of its size (1.19 Å) relative to Ca (1.0 Å), but a smaller dilation than was observed for Ba, also consistent with its size relative to Ba (1.35 Å). Finally, we note that no Pb-Pb backscattering was identified.

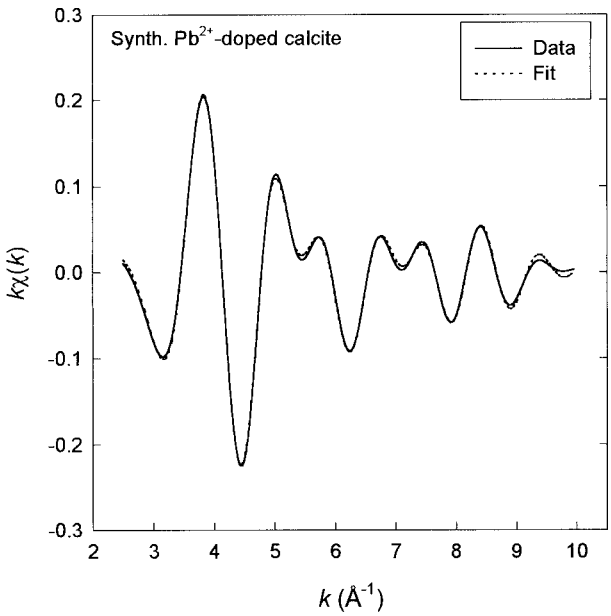

FIGURE 8. The *k*-space representation of the fit (dashed line) to raw data (solid line) for the synthetic Pb-doped calcite. Fitting was done in *R* space.

DISCUSSION

Substitution mode in calcite

Our XAFS results provide direct confirmation that Co^{2+}, Zn^{2+}, Pb^{2+}, and Ba^{2+}, with sizes either significantly smaller or larger than host Ca^{2+}, substitute in the Ca site in the calcite structure with varying amounts of local distortion. Moreover, our finding that the local environment of each trace element (except Ba^{2+}) is the same in both synthetic and natural calcite samples suggests this to be the dominant substitution mode for most trace-element-containing calcites. There is little surprise that trace Co^{2+} ($^{[6]}r$ = 0.745 Å) and Zn^{2+} ($^{[6]}r$ = 0.74 Å) are accommodated in the sixfold coordinated Ca site, despite the facts that their ionic radii are 25% smaller than that of Ca^{2+} ($^{[6]}r$ = 1.00 Å) and solid solution in the $CaCO_3$-$CoCO_3$ and $CaCO_3$-$ZnCO_3$ joins is extremely limited at low temperatures (cf. Goldsmith 1983). It is well known that ions smaller than a host may be readily accommodated at low concentrations. This is not so evident for Pb^{2+} and Ba^{2+}, however, which are larger than host Ca ($^{[6]}r_{Pb^{2+}}$ = 1.19 Å; $^{[6]}r_{Ba^{2+}}$ = 1.35 Å), form end-member carbonates having the aragonite structure at ambient temperature, and rarely occur in sixfold coordination as major constituents. In fact, Pingitore (1986) interpreted his Ba coprecipitation results to suggest that Ba is not accommodated in the octahedral Ca site, and instead they favored a defect substitution site. Our XAFS results for the synthetic Ba-containing calcite clearly demonstrate substitution in the Ca site, although not without significant local distortion. In contrast, in the natural Ba-rich calcite from the Långban carbonatite, the Ba occurs dominantly as a second phase impurity ($BaSO_4$).

Our finding of Pb^{2+} substitution at the Ca site is consistent with the X-ray standing wave results of Qian et al. (1994) and Sturchio et al. (1997) who showed that aqueous Pb^{2+} exchanges dominantly with Ca at the calcite surface. Moreover, the XAFS study of Pingitore et al. (1992) showing the incorporation of Sr^{2+} ($^{[6]}r_{Sr^{2+}}$ = 1.17 Å) at the Ca site in calcite suggests the same mode for the similarly sized Pb^{2+}. A point worth emphasizing here is that these substitution modes (i.e., in the octahedral Ca site) exist for trace and minor concentration levels, whereas this may not be the case at higher concentrations.

Surface incorporation sites vs. bulk sites

We noted earlier that our synthetic trace-element-containing calcite crystals grew by advance of nonequivalent growth steps at which trace elements were incorporated differentially into structurally distinct surface sites (Paquette and Reeder 1995; Reeder 1996). Our XAFS results allow us to conclude that, for the case of growth on the $\{10\bar{1}4\}$ faces of calcite, the presence of multiple surface sites does not result in different local environments for the trace elements after their "burial" into the bulk structure during growth. Once the impurity cation attaches at the surface site, addition of subsequent growth units (i.e., CO_3 anions) completes the coordination sphere around the impurity as it does around Ca, but with some distortion. This indicates that the differences in coordination geometry that distinguish the different surface Ca sites are subtle, able to cause differences in the amount of incorporation but not able to effect changes in coordination for imperfectly sized impurity ions.

Is there clustering of trace metal ions?

The calcite crystals studied here may be considered as dilute substitutional solid solutions. Even though the trace metal distributions are not strictly uniform throughout the crystals, our XAFS results failed to show any indication of backscattering from an atom of the same type as the absorber, i.e., Co-Co, Zn-Zn, etc. Therefore, we may conclude that in the bulk crystal the nearest cation neighbors for each trace element are Ca atoms (excluding C), and no significant clustering of the trace metal occurs on the length scale corresponding to the fourth coordination shell in the calcite structure, i.e., 4–5 Å.

Distortion and relaxation around impurity ions

An isovalent substitution of an ion necessarily creates some distortion of the structure if its size differs from that of the host: a local contraction for smaller ions and a dilation for larger ions. The extent to which the structure adjusts to the size of the ion was described as the compliance of the site by Dollase (1980), who concluded that various structures, depending on their topology and coordination, may exhibit different tendencies to resist collapse or dilation around the substituent. The magnitude of such distortions and the distance over which they extend are important parameters affecting the stability and reactivity of solid solutions, and they clearly have a bearing on the magnitude of equilibrium partitioning of trace elements.

Martins and Zunger (1984) and Boyce and Mikkelsen (1985) provided similar views of the variation of bond lengths around isovalent substituents in simple binary solid solutions. The important finding of their experimental studies is that the actual first-shell bond distance (i.e., as determined by XAFS) around a substituting ion is not invariant with composition in the compound but shows a small, progressive change over the composition range of the substitution (Fig. 9). They noted that this behavior falls between two extremes, one in which the interatomic distance may be considered invariant over the composition range of substitution (sometimes referred to as the Pauling limit, reflecting one viewpoint that bond distance should be a conservative property), and the other represented by Vegard's law (also known as the virtual crystal approximation) in which actual distances correspond to a weighted average of distances in the pure end-members. XAFS results, mostly for binary semiconductors but also for a few alkali halides and oxides, indicate that some variation in first-shell distance with composition is always observed, but not so great that Vegard's law behavior is ever closely approached.

Our XAFS results allow determination of site compliances for both large and small impurities in calcite and comparison with other binary solutions, but only for the very dilute case. In view of the findings of Martins and Zunger (1984) and Boyce and Mikkelsen (1985), one would predict that first-shell Co-O and Zn-O distances should lie between their corresponding distances in $CoCO_3$ and $ZnCO_3$ and the Ca-O distance in calcite. For trace concentrations of Pb and Ba in calcite, first-shell Pb-O and Ba-O distances should be less than their values in hypothetical calcite-structured $PbCO_3$ and $BaCO_3$ but greater than the Ca-O distance in calcite.

First-shell distances

A consistent observation for both the Co- and Zn-containing calcite samples is that first-shell M-O distances are only very slightly longer than corresponding distances in their respective end-member carbonates: 2.14–2.16 Å in the Co-doped calcites vs. 2.110 Å in $CoCO_3$, and 2.14–2.15 Å in the Zn-doped calcites vs. 2.111 Å in $ZnCO_3$. In contrast, these distances are much smaller than the Ca-O distance in calcite (2.360 Å) (Fig. 10). And hence for Co and Zn we can conclude that the polyhedral linkage of calcite shows little resistance to collapse around these small impurities. The site compliance for both Co and Zn is large, 80–90% in both cases. Although con-

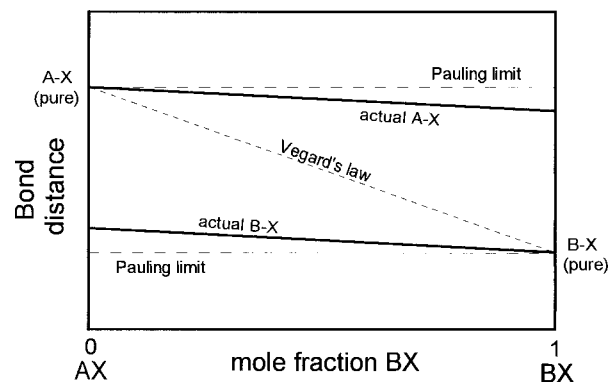

FIGURE 9. Schematic diagram showing possible trends of actual first-shell M-X bond distances for a binary solid solution (AX-BX). The Pauling limit lines (dashed) correspond to individual bond distances that are invariant with composition of the solid solution, whereas a composition-weighted average of these gives a continuous variation with composition (for both A-X and B-X) that is consistent with Vegard's law behavior. XAFS studies (see text) indicate that actual M-X distances (solid lines) lie somewhere between these extremes and deviate most from the Pauling limit at dilute compositions (e.g., the A-X distance in nearly pure BX). Our observations for trace elements in calcite relate exclusively to this dilute composition region, yet show that the actual M-O distances are much closer to values given by the Pauling limit than by Vegard's law. (Modified from Martins and Zunger 1984.)

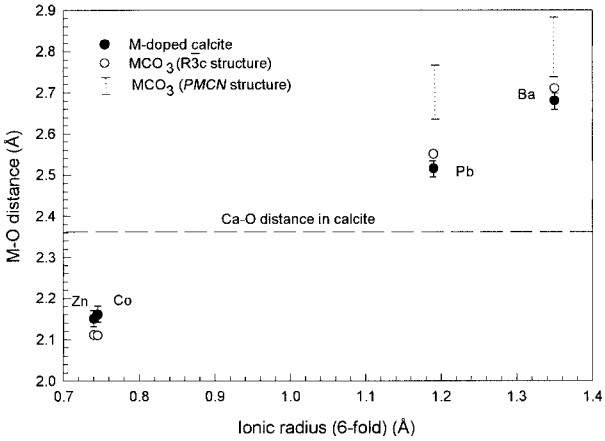

FIGURE 10. Observed first-shell M-O distances (solid circles) in the synthetic M-doped calcites plotted as a function of ionic radius of the impurity M. Open circles are M-O distances in the respective pure MCO_3 compounds with the calcite structure ($R\bar{3}c$); values for $PbCO_3$ and $BaCO_3$ are the sum of appropriate ionic radii (see text) and agree with values extrapolated from data for known $R\bar{3}c$ structures. The M-O distances for the metal impurities are only slightly greater (Co and Zn) or slightly less (Pb and Ba) than corresponding distances in the respective pure rhombohedral metal carbonates. For comparison, the ranges are shown for first-shell Pb-O and Ba-O distances in the orthorhombic $PbCO_3$ and $BaCO_3$ structures (*Pmcn*).

sistent with the model described by Martins and Zunger (1984) and Boyce and Mikkelsen (1985), the large compliances indicate a large deviation from a Vegard's law type behavior for first-shell distances (Fig. 9). Therefore, at a microscopic scale, the notion that a substituting ion smaller than the host necessarily occupies a "large site" may not always be justified.

Similar comparisons for Pb and Ba in calcite are hindered by the lack of end-member Pb and Ba carbonates with the calcite structure. However, good estimates can be obtained for Pb-O and Ba-O distances in hypothetical calcite-structure end-members by using the sum of the appropriate ionic radii (Shannon 1976); such sums agree well with measured distances for actual calcite-structure carbonates. This yields a Ba-O distance of 2.71 Å in a hypothetical rhombohedral $BaCO_3$ and hence a site compliance of ~90% for the Ba-doped calcite. We also noted earlier that the Ba-O distance (2.66 Å) in the high-temperature rhombohedral form of $BaCO_3$, in which the Ba is in octahedral coordination, is very close to that in the Ba-doped calcite. Using that estimate yields a site compliance of ~100%. The estimated Pb-O distance for a rhombohedral $PbCO_3$ given by the sum of ionic radii is 2.55 Å, which yields a site compliance of ~85% for Pb^{2+} in calcite. Alternative estimates of Ba-O and Pb-O distances using known values in the few compounds in which Pb^{2+} and Ba occur as major constituents in octahedral coordination also yield large compliances, consistently greater than 75%.

The significance of these large compliances is shown in Figure 10 where it is seen that the first-shell distances are shifted only very slightly toward the value of the Ca-O distance in calcite (2.36 Å), a nominal measure of the size of unsubstituted octahedra in the calcite structure. Within the errors of the distances, the compliance values all lie within the same range and are essentially independent of the size of the substituent; therefore compliances must be characteristic of the structure. We note, however, that the Sr-O distance in Sr^{2+}-doped calcite determined by Pingitore et al. (1992) does not seem to agree well with the systematic behavior shown here. The Sr-O distance predicted for a rhombohedral $SrCO_3$ using the sum of appropriate ionic radii (1.18 + 1.36 = 2.54 Å) is shorter than their XAFS-determined Sr-O distance (2.58 ± 0.03 Å), rather than longer (as was the case for Pb and Ba in calcite). Hence, calculation of the site compliance gives a value greater than 100%. Despite the obvious uncertainty, we believe it is reasonable to assume that the actual site compliance for Sr is large.

The XAFS results presented by Waychunas et al. (1994) for substitution of Fe^{2+} in MgO is one of the few systematic studies of bond length variation with composition for a simple oxide structure. The dilute Fe^{2+} portion of their work offers a useful comparison for the present results. Their observed Fe-O distance for approximately 1 mol% Fe in MgO is ~0.03 Å shorter than the Fe-O distance in "pure" FeO, corresponding to a site compliance of 50%, which is smaller than the range of compliance values for calcite. The EXAFS results of Boyce and Mikkelsen (1985) for the RbBr-KBr solid solution, also having the rocksalt structure, show a compliance for the cation site of about 54%. Vernon and Stearns' (1984) XAFS data for Sr substitution in fluorite indicate a compliance of 60% at the Ca site. For anion substitution in rocksalt halides, the XAFS study by Sato et al. (1992) for the RbCl-RbBr binary and the study by Boyce and Mikkelsen (1985) for the RbI-RbBr binary both show compliances of about 60%. All these compliance values are consistently smaller than the range of values for the Ca site in calcite.

On the basis of distance-least-squares modeling Dollase (1980) proposed that site compliance should be controlled by connectivity of the structure, and particularly the coordination of the nearest neighbors of the impurity. Our present results support this view. The greater compliance for substitution in calcite relative to the rocksalt structure reflects their different topologies. Polyhedra in the rocksalt structure are exclusively edge sharing, whereas in calcite they are exclusively corner sharing. Edge sharing also dominates in the fluorite structure. The greater flexibility afforded the corner-sharing topology in calcite is apparently expressed as a higher site compliance for substitution. Furthermore, the high compliance values we observed for the calcite structure (80–90%) are consistent with Dollase's predicted inverse correlation between site compliance and coordination number of the ligand; a coordination number of 3 (for oxygen in calcite) corresponds to a compliance of approximately 80%.

Galoisy et al. (1995) also found that the XAFS-determined mean $Ni^{[M1]}$-O distance in San Carlos olivine is similar to that in end-member Ni_2SiO_4 and shorter than the mean M1-O distance in Mg_2SiO_4. Although the actual difference in this example is very small (0.016 Å), it also suggests a large compliance. All these findings emphasize that actual distortions at imperfectly sized impurities are not represented well by X-ray diffraction studies, which average over different atom

types at a given site. As a consequence, Vegard's law-type behavior for interatomic distances in a solid solution does not hold at a microscopic scale.

Higher shells

The dilation or contraction around the impurity diminishes with increasing radial distance from the impurity. We can gain some insight to this relaxation field by comparing observed distances in all the coordination shells for the impurity with the corresponding distances around Ca in pure calcite. In Figure 11, the value $R - R_0$, the difference between the observed shell distance (R) and the corresponding value in calcite (R_0), is plotted as a function of shell distance (R) from the trace impurity (i.e., the absorber). In this type of plot, the value $R - R_0 = 0$ corresponds to an absence of distortion. Hence, with increasing distance from the trace metal, $R - R_0$ values should tend toward zero. This behavior is indeed shown for all the trace metals in calcite, although the trend line for Ba remains displaced well above a value of zero even at the most distant shell that we fitted at ~4.0 Å). This fourth shell is composed of the nearest Ca neighbors (at 4.048 Å in calcite, Table 3) and gives the separation between centers of unlike octahedra (M vs. Ca) shared at one corner. Figure 12 compares the observed M-Ca distances of the trace-metal-containing calcites with corresponding M-M distances in both the rhombohedral and orthorhombic MCO_3 structures. The observed M-Ca distances for all the metal-doped calcites are much nearer the 4.048 Å distance in calcite than to corresponding values in their respective pure carbonates with the calcite structure (or with the orthorhombic structure for Ba and Pb).

By inspection of the overall trends in Figure 11, we can estimate that most of the relaxation is confined within a radial distance of 6–7 Å from the metal. If this is the case, the region that is significantly affected by structural distortion around an impurity may be extremely limited in calcite. We note, however, that, within the estimated errors of the fitted distances,

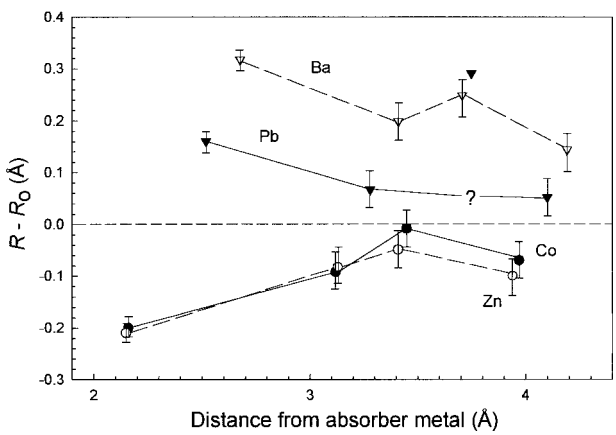

FIGURE 11. Deviation of the observed absorber-shell distance (R) from the corresponding shell distance in ideal calcite (R_0) plotted as a function of (radial) distance from the metal absorber. The trend lines are not smooth but indicate a convergence to an undistorted structure, perhaps within 6–7 Å of the impurity.

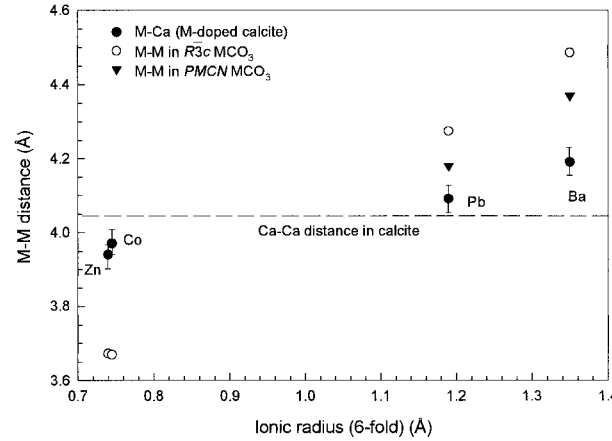

FIGURE 12. Observed M-Ca distances (solid circles) in the synthetic M-doped calcites plotted as a function of ionic radius of the impurity M. Open circles are the corresponding M-M distances in the pure MCO_3 compounds with the calcite structure ($R\bar{3}c$); values for $PbCO_3$ and $BaCO_3$ are extrapolated from the trend of known $R\bar{3}c$ structures. The M-Ca distances are closer to the Ca-Ca distance in ideal calcite than to corresponding distances in their respective pure metal carbonates. Triangles give the shortest M-M distances in orthorhombic $PbCO_3$ and $BaCO_3$, which fall between values in the rhombohedral structures.

the relaxation shown by successive shells does not appear to be a smooth function of radial distance. (Here we have excluded the third shell in the trend for Pb because of the ambiguity noted earlier.) This is consistent with the behavior predicted by Dollase (1980) and reflects partly that the displacements in a real structure are transmitted though bonds, whose directions, depending on the structure, will generally not be co-linear. Hence, displacements are not transmitted uniformly as a function of radial distance alone. In the calcite structure, the first three atomic shells around the Ca site are all associated with the six nearest-neighbor CO_3 groups. Because the CO_3 groups behave as rigid units (Reeder 1983), the observed displacements within the first three atomic shells almost certainly include a small component of rotation or tilting of the CO_3 unit. This may contribute to the irregularities in the relaxation trend.

Bulk structural controls on substitution and relaxation behavior

These observations for Pb and particularly for Ba emphasize the fact that as a substitutional impurity a metal cation may occur in a coordination environment in which it rarely occurs as a major constituent, and it may substitute for a species that is of significantly different size. Such behavior (including the high compliance) may be favored by the calcite structure (Fig. 13) because of the ready modes of tilting and bending at shared corners of polyhedra. We believe the corner-sharing topology of calcite is one of the primary reasons that calcite shows such a wide variety of substitutions at trace and minor concentration levels, among them both small (e.g., Mg, Co, and Ni) and large (e.g., Pb, Sr, and Ba) divalent metals.

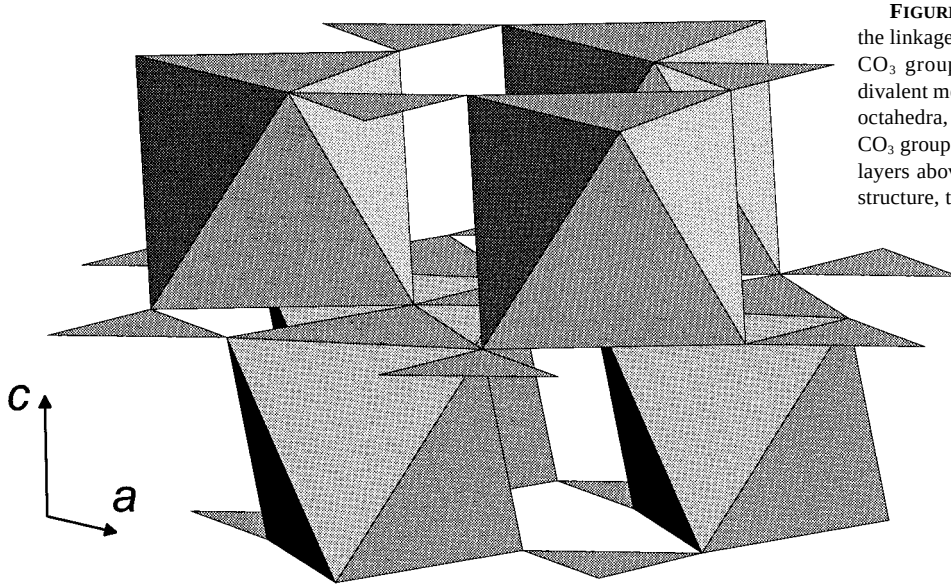

FIGURE 13. Polyhedral drawing showing the linkage of the CaO_6 octahedra and planar CO_3 groups in the calcite structure. The divalent metal impurities substitute in the Ca octahedra, which share corners with planar CO_3 groups and neighboring octahedra from layers above and below. Unlike the rocksalt structure, there is no edge sharing in calcite.

CONCLUDING REMARKS

Because previous studies have clearly shown that the extent of incorporation of trace elements into calcite during growth from aqueous solutions is controlled by structural aspects of surface sites (e.g., Reeder and Rakovan 1999 and references therein), our focus on bulk sites here should not be construed to indicate that aspects of distortion and relaxation at sites in the bulk structure are necessarily the primary controls on experimental K_d values. Nevertheless, these factors may play some role in retention of a metal impurity as it is buried by successive layers, during which time the filled surface site is transformed into a site in the crystal interior. However, the compliance and relaxation that we have considered for bulk sites must have a corresponding (although presumably different) manifestation at surface sites (cf. Cheng et al. 1998); it may then be likely that surface sites could differ in their compliance and so have different tendencies for incorporation or adsorption of impurities.

And finally, we note the recent advances in modeling trace-element partitioning between melt and crystal by consideration of the elastic strain associated with substitution (e.g., Blundy and Wood 1994). The present study indicates that the strain around an impurity may not be determined solely by the "size" of the substituting ion; rather the compliance of the site also plays a significant role.

ACKNOWLEDGMENTS

We thank L. Fareria and K. Pandya for assistance at NSLS. We also thank D. Xirouchakis and D.H. Lindsley for kindly synthesizing CoO and $CoCO_3$, respectively. A Co-bearing calcite (Peramea, Spain) was provided by the National Museum of Natural History, Smithsonian Institution, and the natural Ba-containing calcite (Långban, Sweden) was provided by E.S. Grew. Critical reviews by Neil Sturchio, Glenn Waychunas, and an anonymous reviewer improved the presentation. This project was supported by NSF grants EAR940546 and EAR9706012.

REFERENCES CITED

Blundy, J.D. and Wood, B.J. (1991) Crystal-chemical controls on the partitioning of Sr and Ba between plagioclase feldspar, silicate melts, and hydrothermal solutions. Geochimica et Cosmochimica Acta, 55, 193–209.

——(1994) Prediction of crystal-melt partition coefficients from elastic moduli. Nature, 372, 452–454.

Boyce, J.B. and Mikkelsen, J.C. (1985) Local structure of ionic solid solutions: Extended x-ray absorption fine structure study. Physical Review B, 31, 6903–6905.

Busenberg, E. and Plummer, L.N. (1985) Kinetic and thermodynamic factors controlling the distribution of SO_4^{2-} and Na^+ in calcites and aragonites. Geochimica et Cosmochimica Acta, 49, 713–725.

Cheng, L., Sturchio, N.C, Woicik, J.C., Kemner, K.M., Lyman, P.F., and Bedzyk, M.J. (1998) High-resolution structural stufy of zinc ion incorporation at the calcite cleavage surface. Surface Science, 415, L976–L982

Chevrier, G., Giester, G., Heger, G., Jarosch, D., Wildner, M., and Zemann, J. (1992) Neutron single-crystal refinement of cerrusite, $PbCO_3$, and comparison with other aragonite-type carbonates. Zeitschrift für Kristallographie, 199, 67–74.

de Villiers, J.P.R. (1971) Crystal structures of aragonite, strontianite, and witherite. American Mineralogist, 56, 758–767.

Dollase, W.A. (1980) Optimum distance model of relaxation around substitutional defects. Physics and Chemistry of Minerals, 6, 295–304.

Effenberger, H., Mereiter, K., and Zemann, J. (1981) Crystal structure refinements of magnesite, calcite, rhodochrosite, siderite, smithsonite, and dolomite, with discussion of some aspects of the stereochemistry of calcite type carbonates. Zeitschrift für Kristallographie, 156, 233–243.

Galoisy, L., Calas, G., and Brown, G.E. (1995) Intracrystalline distribution of Ni in San Carlos olivine: An EXAFS study. American Mineralogist 80, 1089–1092.

Gnanapragasam and Lewis (1995) Elastic strain energy and the distribution coefficient of radium in solid solutions with calcium salts. Geochimica et Cosmochimica Acta, 59, 5103–5111.

Goldsmith, J.R. (1983) Phase relations of the rhombohedral carbonates. Reviews in Mineralogy, 11, 49–76.

Haskel, D., Ravel, B., Newville, M., and Stern, E.A. (1995) Single and multiple scattering XAFS in $BaZrO_3$: A comparison between theory and experiment. Physica B, 208/209, 151–153.

Hill, R.J. (1987) Structure of $PbSb_2O_6$ and its relationship to the crystal chemistry of PbO_2 in antimonial lead-acid batteries. Journal of Solid State Chemistry, 71, 12–18.

Hyde, B.G. and Andersson, S. (1989) Inorganic crystal structures, p. 257–271. Wiley, New York.

Kitano, Y., Kanamori, N., and Oomori, T. (1971) Measurement of the distribution coefficients of strontium and barium between carbonate precipitate and solution. Geochemical Journal, 4, 183–206.

Lamble, G.M., Reeder, R.J., and Northrup, P.A. (1997) Characterization of heavy

metal incorporation in calcite by XAFS spectroscopy. Journal de Physique IV, Supplement 7, C2, 793–797.

Losilla, E.R., Aranda, M.A.G., Ramirez, F.J., and Bruque, S. (1995) Crystal structure and spectroscopic characterization of MAs_2O_6 (M = Pb, Ca). Two simple salts with AsO_6 groups. Journal of Physical Chemistry, 99, 12975–12979.

Mahe, R. (1967) Etude structurale du metaniobate du plomb rhomboedrique. II. Positions des atomes. Bulletin Societe de Chimique France, 1967, 1879–1884.

Martins, J.L. and Zunger, A. (1984) Bond lengths around isovalent impurities and in semiconductor solid solutions. Physical Review B, 30, 6217–6220.

Moore, P.B., Sen Gupta, P.K., Shen, J., and Schlemper, E.O. (1991) The kentrolite-melanotekite series, $4Pb_2(Mn,Fe)_2^{3+}O_2[Si_2O_7]$: Chemical crystallographic relations, lone-pair splitting, and cation relation to $8URe_2$. American Mineralogist, 76, 1389–1399.

Morse, J.W. and Bender, M.L. (1990) Partition coefficients in calcite: Examination of factors influencing the validity of experimental results and their application to natural systems. Chemical Geology, 82, 265–277.

Mucci, A. and Morse, J.W. (1983) The incorporation of Mg^{2+} and Sr^{2+} into calcite overgrowths: influences of growth rate and solution composition. Geochimica et Cosmochimica Acta, 47, 217–233.

———(1990) Chemistry of low-temperature abiotic calcites: Experimental studies on coprecipitation, stability, and fractionation. Aquatic Sciences, 3, 217–254.

Newville, M., Ravel, B., Haskel, D., Stern, E.A., and Yacoby, Y. (1995) Analysis of multiple scattering XAFS data using theoretical standards. Physica B, 208/209, 154–156.

Paquette, J. and Reeder, R.J. (1990) New type of compositional zoning in calcite: Insights into crystal-growth mechanisms. Geology, 18, 1244–1247.

———(1995) Relationship between surface structure, growth mechanism, and trace element incorporation in calcite. Geochimica et Cosmochimica Acta, 59, 735–749.

Pertlik, F. (1986) Structures of hydrothermally synthesized cobalt(II) carbonate and nickel(II) carbonate. Acta Crystallographica, C42, 4–5.

Pingitore, N.E. Jr. (1986) Modes of coprecipitation of Ba^{2+} and Sr^{2+} with calcite. In J.A. Davis and K.F. Hayes, Eds.,Geochemical processes at mineral surfaces, p. 574–586. American Chemical Society Symposium 323, Washington, D.C.

Pingitore, N.E., Lytle, F., Davies, B.M., Eastman, M.P., Eller, P.G. and Larson, E.M. (1992) Mode of incorporation of Sr^{2+} in calcite: Determination by X-ray absorption spectroscopy. Geochimica et Cosmochimica Acta, 56, 1531–1538.

Qian, Y., Sturchio, N.C., Chiarello, R.P., Lyman, P.F., Lee, T.-L., and Bedzyk, M.J. (1994) Lattice location of trace elements within minerals and at their surfaces with X-ray standing waves. Science, 265, 1555–1557.

Reeder, R.J. (1983) Crystal chemistry of the rhombohedral carbonates. Mineralogical Society of America Reviews in Mineralogy, 11, 1–47.

———(1996) Interaction of divalent cobalt, zinc, cadmium, and barium with the calcite surface during layer growth. Geochimica et Cosmochimica Acta, 60, 1543–1552.

Reeder, R.J. and Rakovan, J. (1999) Surface structural controls on trace element incorporation during crystal growth. In B. Jamtveit and P. Meakin, Eds., Growth, dissolution, and pattern formation in geosystems. Kluwer, Dordrecht.

Rehr, J.J., Zabinsky, S.I., and Albers, R.C. (1992) High-order multiple scattering calculations of x-ray-absorption fine structure. Physical Review Letters, 69, 3397–3400.

Sasaki, S., Fujino, K., and Takeuchi, Y. (1979) X-ray determination of electron-density distributions in oxides, MgO, MnO, CoO, and NiO, and atomic scattering factors of their constituent atoms. Proceedings of the Japan Academy, 55, 43–48.

Shannon, R.D. (1976) Revised effective ionic radii and systematic studies of interatomic distances in halides and chalcogenides. Acta Crystallographica, A32, 751–767.

Strømme, K.O. (1975) On the crystal structures of the high-temperature forms of the strontium and barium carbonate and structurally related compounds. Acta Chemica Scandinavica, 29, 105–110.

Sturchio, N.C., Chiarello, R.P, Cheng, L., Lyman, P.F., Bedzyk, M.J., Qian, Y., You, H., Yee, D., Geissbuhler, P., Sorensen, L.B., Liang, Y., and Baer, D.R. (1997) Lead adsorption at the calcite-water interface: Synchrotron X-ray standing wave and X-ray reflectivity studies. Geochimica et Cosmochimica Acta, 61, 251–263.

Sturchio, N.C., Antonio, M.R., Soderholm, L., Sutton, S.R., and Brannon, J.C. (1998) Tetravalent uranium in calcite. Science, 281, 971–973.

Waychunas, G.A., Dollase, W.A., and Ross, C.R. (1994) Short-range order measurements in MgO-FeO and $MgO-LiFeO_2$ solid solutions by DLS simulation-assisted EXAFS analysis. American Mineralogist, 79, 274–288.

Zabinsky, S.I., Rehr, J.J., Ankudinov, A., Albers, R.C., and Eller, M.J. (1995) Multiple-scattering calculations of X-ray absorption spectra. Physical Review B, 52, 2995–3009.

MANUSCRIPT RECEIVED JULY 7, 1998
MANUSCRIPT ACCEPTED FEBRUARY 13, 1999
PAPER HANDLED BY GLENN A. WAYCHUNAS